Elastic softening in the rotator phase of the perfluoroalkane $C_{24}F_{50}$

R. Jiménez, J. K. Krüger, C. Fischer, and K.-P. Bohn
Fachrichtung Experimentalphysik 10.2, Universität des Saarlandes, Bau 38, Postfach 151150, D-66041 Saarbrücken, Germany

V. Dvorák and J. Holakovský
Institute of Physics of the Czech Academy of Sciences, Na Slovance 2, 18040 Prague 8, Czechoslovakia

P. Alnot
Laboratoire Central de Recherche (LCR), Thomson CSF, F-91404 Orsay, Cedex, France
(Received 3 June 1994; revised manuscript received 20 October 1994)

The rotator phase of $C_{24}F_{50}$ has been characterized in its calorimetric as well as in its elastic properties. To perform the elastic characterization we took advantage of a polytetrafluoroethylene-induced-alignment crystal-growth technique. Special interest is paid to the rotator phase and the premelting behavior therein as reflected by the elastic stiffness coefficients c_{33} and c_{44}. The anomalous elastic behavior is interpreted in the frame of the Landau theory. The premelting process is related to molecular conformational defects.

I. INTRODUCTION

Their specific rotator phases (premelting phases), their intricate phase transition behavior, and their model character for related polymers are some of the reasons that make the linear telomers (oligomers), like *n*-paraffins, perfluoroalkanes, etc., subjects of great physical interest. Numerous investigations (e.g., Refs. 1–3) have been made of the physical properties of the crystalline state of *n*-paraffins and perfluoroalkanes with their specific anisotropic inter- and intramolecular interactions and defects which are of fundamental interest for the understanding of the phenomenological properties of related macromolecular materials.

The mechanical properties, including the elastic anisotropy, of telomer crystals consisting of linear-chain molecules are drastically influenced by the arrangement of covalent bonds within the chain molecules as well as by the weak intermolecular interactions.[4,5] In turn, the findings about the static and dynamic elastic properties of these materials contribute to the understanding of the interrelations between their molecular structure, molecular dynamics, and morphology on one hand, and their outstanding phenomenological properties on the other.

Unfortunately, the determination of the elastic properties of crystalline telomers is a difficult task.[3] The tendency of this material class to show polymorphism and polytypism makes it difficult to grow sufficient defectless single crystals;[6] moreover, habit and plasticity of solution and melt-grown samples make it difficult to prepare crystal cuts suitable for ultrasonic and/or Brillouin measurements. Despite all these problems there exists some preliminary work devoted to the description of the elastic behavior of this substance class that is mainly based upon indirect experimental methods.

The temperature dependence of the shear stiffness of several *n*-paraffins in the polycrystalline state was successfully measured by Pechhold, Dollhopf, and Engel.[7] However, the relation between these shear stiffnesses and those of the single-crystalline state is not evident.

Heyer, Bucheneau, and Stamm[8] were able to determine the elastic shear constants of polyethylene microcrystals by using inelastic neutron scattering (INS). This method, developed by Buchenau[9] for application to polycrystalline samples, is based on a statistical treatment of intensity profiles. It has the advantage that no single crystals are needed to determine the elastic properties. However, scattering intensities must be carefully corrected for the spectrometer resolution function and for background scattering. The accuracy obtained with this method is much inferior to that reached by measurements of phonon-dispersion curves on single crystals. Furthermore, since INS measures the elastic constants at frequencies in the THz range, remarkable differences compared to low-frequency elastic data are to be expected.

Longitudinal-acoustic mode (LAM) frequencies of different orders of $C_{33}H_{68}$ measured by Raman spectroscopy were used by Strobl and Eckel[1] in order to estimate several elastic constants at room temperature. Krüger and co-workers[10,11] succeeded in measuring directly several elastic stiffness constants of solution grown Hexatriacontane ($C_{36}H_{74}$) single crystals as a function of temperature, using Brillouin spectroscopy. Results were also successfully obtained applying the Brillouin spectroscopy to determine the temperature behavior of some elastic constants in the rotator phase of $C_{16}F_{34}$ and $C_{20}F_{42}$.[4,12] In both cases advantage was taken of the 90A- and 90R-scattering geometries[13–15] which allow measurements on crystal plates of only a few micrometers thickness. From their investigations within the rotator phase, an unexpectedly strong decrease of the stiffness modulus c_{33} (propagation of the longitudinal sound mode normal to the crystalline layers) with increasing temperature resulted. Furthermore, no shear stiffness coefficient c_{44} ($=c_{55}$) was found within this phase, suggesting the possibility that the corresponding shear modes become extremely

 ©1995 The American Physical Society

soft because of a very weak interlayer coupling indicating the possibility of premelting. Unfortunately, the rotator phases of n-paraffins exist only in narrow temperature intervals, which even decrease with increasing molecular chain length.

In order to get more insight into the premelting process within the rotator phases indicated by the slowing down of c_{33} of $C_{36}H_{74}$, attention has been focused on fully fluorine substituted n-alkanes (perfluoroalkanes, C_nF_{2n+2}) which show rotator phases spread over a much larger temperature range as in the case of n-paraffins. As a result, anisotropy inversion of the longitudinal moduli was found in the rotator phase of $C_{16}F_{34}$ and $C_{20}F_{42}$; in addition an unexpected premelting transition was found in $C_{20}F_{42}$ by Marx, Krüger, and Unruh.[4] A theoretical explanation of this premelting transition was given by Dvorák[16] recently. It seems that the inter-lamellar regions formed by the endgroups of the carbon chains between neighbor lamellae play an important role in the set in of the premelting process. Indeed the telomer chains in the lamellae present several components of disorder in the rotator phase that make it very difficult to define stable inter-lamellar regions.[17–19]

In the context of these studies on perfluoroalkanes[4,12] and semifluorinated alkanes[5] an efficient Brillouin technique was applied which allows, at least in principle, the determination of the complete elastic stiffness tensor from mesoscopic single crystalline domains of a polydomain filmlike sample. For reasons of simplicity we call this technique the thin-film-domain (TFD) technique. The main difficulty of the TFD technique is the adjustment of suitable, sufficiently representative, domains for Brillouin measurements.[12]

The aim of the current paper is to characterize the elastic properties in the rotator phase of $C_{24}F_{50}$ and interpret them in context with the elastic behavior in the rotator phase of $C_{16}F_{34}$ and $C_{20}F_{42}$,[4] especially with reference to the universal premelting behavior also observed in n-alkanes.[20] To obtain the elastic constants of $C_{24}F_{50}$ we will take advantage of a new technique for the preparation of highly oriented crystal mats of linear telomers, which allows the determination of virtually all coefficients of the elastic stiffness tensor of this material class. This so-called polytetrafluoroethylene-induced-alignment (PIA) technique, introduced by Wittmann and Smith,[21] has been proved to be a powerful tool to orient semicrystalline polymers[21–23] as well as liquid crystals.[24,25] The premelting behavior will be discussed as being connected to a "continuous" phase transition in the frame of the Landau theory with coupling between strain and order parameter. It will be related to molecular conformational defects. The elastic properties will be compared with those of smectic-B liquid crystals.

II. EXPERIMENT

A. Sample preparation

The PIA technique uses the fact that linear polymer and oligomer molecules tend to align themselves on highly oriented crystalline polytetrafluoroethylene (PTFE) with their molecular chain axes along the unique axis of the PTFE. The method is based on the deposition of a highly oriented and highly crystalline PTFE layer of about 10 nm thickness on a smooth glass surface. The deposition of the layer takes place by rubbing a PTFE rod on a clean glass slide at elevated temperatures, thus mechanically inducing a perfect orientation of the PTFE crystallites with their unique axes pointing along the rubbing direction. Because of their efficient alignment influence on linear polymers[21–23] and related materials, as for example liquid crystals,[24,25] we denote such a supporting PTFE film as PIA substrate.

The growth of a thin crystalline n-telomer film (for instance of $C_{24}F_{50}$ or $C_{20}F_{42}$) on the PIA substrate occurs in such a way that the molecules of the deposited substance show an outstanding unidirectional texture and that the textured thin film consists of a highly textured crystal mat having the crystallographic c axis of the quasihexagonal lattice of the rotator phase[4] aligned along the rubbing direction of the PTFE substrate and possibly one further crystallographic axis within the substrate plane.[20] Until now, there exist only preliminary ideas about the precise transcrystallization mechanisms induced by the PIA substrate.[21]

It is evident that the PIA effect decreases with increasing sample thickness; at a given thickness of a filmlike sample, the PIA effect can be enhanced increasing the effective surface using a PIA-coated glass sandwich as sample holder. The filling procedure of the sandwich cell took advantage of the capillarity effect. Sample thicknesses range typically between 1 and 5 μm. The sample investigated in this work ($C_{24}F_{50}$) was purchased from Aldrich having usual commercial purity grade.

B. Brillouin spectroscopy

Taking advantage of the 90A-scattering geometry[13,26,27] (Fig. 1) one can obtain information about the elastic constants in thin films by means of the Brillouin spectroscopy (BS). Moreover, the use of the angular and space-resolving BS (Refs. 23 and 28) allows the determination of almost all the elastic constants present in the elastic stiffness tensor of the crystalline state using exclusively polydomain filmlike samples. The corre-

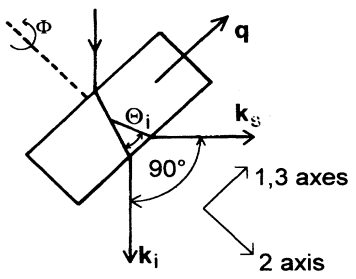

FIG. 1. Schematical representation of the 90A-scattering geometry. $\mathbf{q}$: Phonon wave vector; $\mathbf{k}_i$: wave vector of incident light; $\mathbf{k}_s$: wave vector of scattered light; Θ_i: inner scattering angle; Φ: rotation angle about the 2 axis (for further information see text).

sponding phonon wave vector $\mathbf{q}$ is contained within the PIA-film plane and the relation between sound velocity v^{90A} and the phonon frequency f^{90A} is

$$v^{90A}=\frac{f^{90A}\lambda_0}{\sqrt{2}} \tag{1}$$

where λ_0 is the laser wavelength in vacuum (514.5 nm in our case). As has been discussed elsewhere,[15] the acoustic wavelength depends little, or in many cases not at all, on the optical refraction properties of the sample. The stiffness coefficient c, related to the measured sound frequency, obeys the relation $c=\rho v^2$ where ρ is the mass density of the material. Measuring the phonon frequency for different directions of the $\mathbf{q}$ vector within the film plane and taking into account the relevant symmetry of the sample under study, one can solve the Christoffel's equation (e.g., Ref. 29) yielding the desired stiffness coefficients c_{kl}. The basic relation for the determination of the elastic stiffness tensor $\mathbf{c}$ written in matrix notation is given by

$$\det(\boldsymbol{l}\boldsymbol{c}\boldsymbol{l}^T-\mathbf{E}c'(p,\mathbf{q}))=0 \tag{2}$$

with

$$\boldsymbol{l}=\begin{bmatrix} l_1 & 0 & 0 & 0 & l_3 & l_2 \\ 0 & l_2 & 0 & l_3 & 0 & l_1 \\ 0 & 0 & l_3 & l_2 & l_1 & 0 \end{bmatrix} . \tag{3}$$

$\mathbf{c}=\{c_{kl}\}$ is the fourth-rank elastic tensor in shortened 6×6 Voigt's notation. It is in general a complex tensor and these equations hold strictly only if the condition $c'\gg c''$ between real part (c') and imaginary part (c'') is fulfilled. $\mathbf{E}$ is a 6×6 unity matrix. l_i ($i=1,2,3$) are direction cosines which define the direction of the wave vector, $\hat{\mathbf{q}}=(l_1,l_2,l_3)$ and p represents the polarization of the acoustic mode. The right-handed orthogonal coordinate directions $\{1,2,3\}$ have been chosen with the 3 axis pointing along the rubbing direction of the PIA film, the 2 axis is directed orthogonal to the PIA sandwich. For the (1,3) plane $\hat{\mathbf{q}}=(\sin\Phi,0,\cos\Phi)$ holds. At ambient temperature $C_{16}F_{34}$ and $C_{20}F_{42}$ have a trigonal rotator phase which, in this special case, is nearly hexagonal (quasihexagonal). From the elastic point of view the materials behave even completely hexagonal.[12] We have no precise idea about the symmetry of the prototype phase of $C_{24}F_{50}$ yet, but because of the very similar elastic behavior of $C_{16}F_{34}$, $C_{20}F_{42}$, and $C_{24}F_{50}$ (see below) we assume an elastically quasihexagonal behavior for this material. For hexagonal symmetry the elastic stiffness tensor has the following form (Voigt's notation):

$$\begin{bmatrix} c_{11} & c_{12} & c_{13} & & & \\ c_{12} & c_{11} & c_{13} & & 0 & \\ c_{13} & c_{13} & c_{33} & & & \\ & & & c_{44} & & \\ & 0 & & & c_{44} & \\ & & & & & c_{66} \end{bmatrix} \quad \text{with } c_{66}=(c_{11}-c_{12})/2 . \tag{4}$$

Using a cryostat-permitting angle-dependent Brillouin spectroscopy,[3] we were able to determine the elastic stiffness components of $C_{24}F_{50}$ as function of temperature.

C. Calorimetry

Calorimetric investigations were performed with the differential scanning calorimetry (DSC) technique. The DSC systems we used were a Perkin-Elmer DSC2 and a Netzsch DSC200. Because of the vapor pressure mentioned above, it was necessary to use special crucibles. The typical heating-cooling rate used in the experiments was 5 K/min.

III. RESULTS AND DISCUSSION

The temperature range of the rotator phase of $C_{24}F_{50}$, as obtained by the DSC calorimetry (Netzsch DSC200) with a heating rate of 5 K/min, extends over 220 K and is shown in Fig. 2. The rotator phase is delimited by a low-temperature heat flux peak at $T_3=220$ K that indicates a first-order structural phase transition for the low-temperature phase to the rotator phase and a high-temperature heat flux peak at $T_m=460$ K representing the melting transition. In order to account for possible influences of the sealed crucibles on the measurements we performed additional calorimetric investigations. First we cooled down the sample from room temperature with a cooling rate of 5 K/min (Perkin-Elmer DSC2) and found a double specific-heat peak structure as can be seen in Fig. 3. The corresponding temperatures are $T=216.5$ K and $T=212$ K. As revealed by Fig. 3, on heating the sample (heating rate 5 K/min) from below 212 K to room temperature, only one specific-heat anomaly was found at $T_3=220$ K. A further cooling to 200 K at a rate of 5 K/min reproduced the two specific-heat anomalies found during the first cooling run. This undercooling behavior

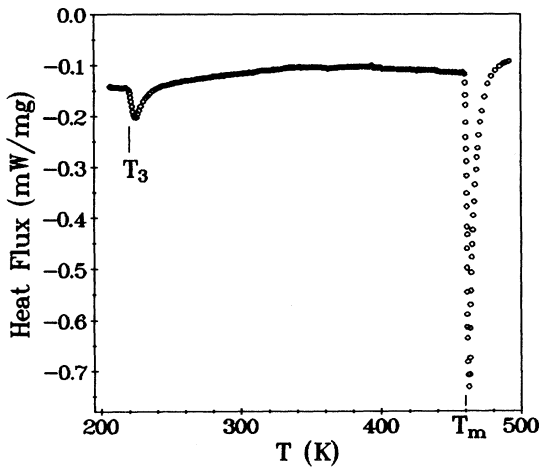

FIG. 2. DSC thermogram (Netsch DSC200) of the rotator phase of $C_{24}F_{50}$ recorded on heating (5 K/min). T_m melting temperature, T_3 transition temperature indicating the transformation from the low-temperature phase to the rotator phase.

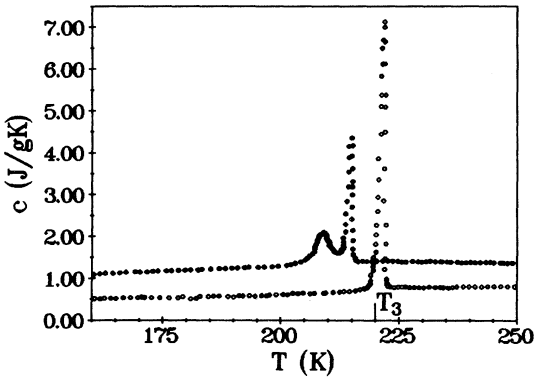

FIG. 3. DSC thermograms of the specific heat c (Perkin-Elmer DSC2) around the low-temperature structural phase transition temperature. Full circles: cooling run. Open circles: heating run (5 K/min heating/cooling rate).

was already found and discussed in detail for $C_{16}F_{34}$ and $C_{20}F_{42}$ (Ref. 4) and indicates the formation of a metastable phase at $T_i = 216.5$ K on cooling from room temperature before the stable low-temperature modification is reached. Similar to the case of $C_{20}F_{42}$, this metastable phase does not appear on heating to ambient temperature.

The study of the elastic behavior of the rotator phase of $C_{24}F_{50}$ was performed on thin-film samples produced in glass sandwiches with PTFE coating (PIA substrate, see Sec. II). To test in a first step the efficiency of the PIA substrate in orienting the $C_{24}F_{50}$ thin film, we performed angular-resolving Brillouin spectroscopy at room temperature ($T \approx 295$ K). Using the $90A$ scattering geometry,[13,14,15,26,27] we guarantee that the phonon wave vector $\mathbf{q}$ always remains in the film plane during sample rotation (see also Fig. 1). A typical Brillouin spectrum for a defined angle Φ is shown in Fig. 4. The complete results are shown in Fig. 5, where the full line represents

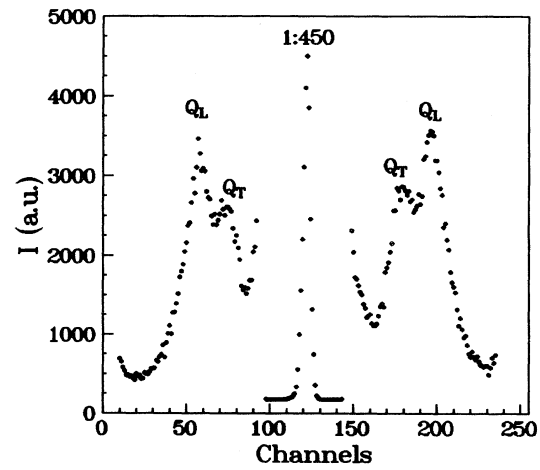

FIG. 4. Brillouin spectrum at $T \approx 295$ K for an angle $\Phi = 32°$. Both the quasilongitudinal (Q_L) and the quasitransverse (Q_T) corresponding phonons are clearly shown. The Rayleigh line was reduced in a factor 450 to fit the graphic scales.

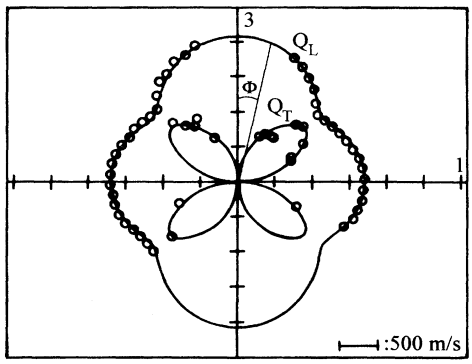

FIG. 5. Sound velocity polar plot of $C_{24}F_{50}$ in the 1–3 plane ($T \approx 295$ K). Circles represent the experimental data. The full line represents the results of the least squares fit of the Christoffel's equation to the experimental data (see also Table I). Q_L: Quasilongitudinal branch; Q_T: Quasitransverse branch; Φ: Angle between $\mathbf{q}$ and 3 axis.

a least-squares fit of the symmetry adapted Christoffel's equation to the experimental data. The elastic indicatrix shows the largest longitudinal sound velocity v_3, along the 3 axis indicating that the c axis of the $C_{24}F_{50}$ crystallites lies within the film plane of the sample and is parallel to the 3 axis. At first approach, this elastic anisotropy of the longitudinal sound velocity is expected because it agrees with that found for PIA-oriented linear polymers[21–23] and liquid crystals[24,25] and linear n-alkanes[20] crystallized on a PIA substrate. In Ref. 20 is demonstrated that the PIA sample is equivalent to a single-crystal plate with the c axis parallel to the crystal surface. The quasitransverse branch goes close to zero along the 1 and 3 axis. However, for reasons of mechanical stability, this mode has to stay definitely nonzero because at the symmetry axes it becomes purely transversal polarized, yielding the shear stiffness c_{44}. However, c_{44} seems to be very small compared to the other stiffness moduli involved in the least-squares fit, suggesting a very weak coupling between adjacent molecular layers of the lamellar crystal. The complete results of the least-squares fit is shown in Table I; the room-temperature value for the density, ρ, was extrapolated from the corresponding values of $C_{16}F_{34}$ and $C_{20}F_{42}$.[4]

We have also investigated the temperature dependence of the main elastic stiffness coefficients using angular-resolving Brillouin spectroscopy. The sample was first measured on heating from room temperature to 450 K, then cooled down to room temperature again and afterwards measured on cooling to 220 K. Due to technical

TABLE I. Elastic stiffness coefficients of $C_{24}F_{50}$ at $T = (295 \pm 1)$ K. The value of the density, ρ, was extrapolated from the room-temperature values given in Ref. 4.

$C_{24}F_{50}$	$T \approx 295$ K $\rho = 2169$ kg/m^3
c_{11} (GPa)	6.33±0.01
c_{33} (GPa)	9.38±0.02
c_{13} (GPa)	1.56±0.02
c_{44} (GPa)	0.04±0.01

reasons, it was not possible to measure below 220 K. The complete results obtained from the polar plot diagrams registered and evaluated at each temperature are shown in Fig. 6. In order to discuss the temperature dependence of the elastic constants, we will proceed first to examine the low-temperature region ($T < 310$ K) and then the high-temperature region ($T > 300$ K). At temperatures below 310 K, the temperature behavior of the elastic stiffness coefficient c_{33} does not correspond to the expected extrapolation of the temperature dependence of the elastic constants measured at higher temperatures ($T > 300$ K). On lowering the temperature, we find an almost temperature independent c_{33} with the particularity that the c_{44} values become clearly larger than zero. Below 250 K, $c_{33}(T)$ closely follows the linear extrapolation of $c_{33}(T)$ (310 K $< T <$ 370 K). $c_{11}(T)$ shows a small steplike anomaly at about 290 K recovering the expected temperature dependence below 250 K. In order to check the reproducibility of this elastic anomaly, we raised the temperature and measured the sound velocity polar diagrams for a second time, at the temperature marked by the numbers 1, 2, and 3 in Fig. 6 (264, 284, and 323 K, respectively). The anomalous elastic behavior was reproduced as well as the usual temperature dependence of the elastic constants for $T > 300$ K. We lowered the temperature again in order to measure the sound velocity polar diagrams at 250 and 220 K (points number 4 and 5 in Fig. 6) reproducing again the anomalous elastic behavior indicating thermoreversibility within the investigated temperature regime.

At this point, we cannot exclude a possible interaction between the PIA substrate and the sample that changes the transition behavior. Of course, the PIA substrate induces a preferential alignment of the $C_{24}F_{50}$ molecular chains, resulting in an orientation of the crystalline c axis parallel to the PTFE rubbing direction (see Sec. II). Although this mechanical interaction between substrate and n-telomer does not influence the structural phase transition temperature from the rotator phase to the low-temperature phase, for instance of $C_{17}H_{36}$,[20] we cannot completely exclude the influence that the PIA substrate has on the appearance or the location of a metastable phase in $C_{24}F_{50}$. The general possibility for the appearance of such a metastable phase on fast cooling has been established by specific-heat measurements (Fig. 3). Therefore, it seems even more likely that the differences of the cooling rates using DSC (5 K/min) and Brillouin spectroscopy (10 K/h), respectively, are responsible for the shift of T_i to almost ambient temperature at slow cooling. As we could not cool our optical cryostat lower than 220 K, we never reached the stable low-temperature phase.

Above 310 K, there exist Brillouin data of the related perfluoroalkanes $C_{16}F_{34}$ and $C_{20}F_{42}$.[4,12] The elastic behavior represented by the elastic stiffness coefficients c_{11}, c_{33}, c_{13}, and c_{44} of $C_{24}F_{50}$ (Fig. 6), obtained recording the polar diagrams and fitting the Christoffel's equation to the experimental data at different temperatures, is very similar to that found in $C_{16}F_{34}$ and $C_{20}F_{42}$. A temperature evolution of the related longitudinal polar diagrams measured in the 1–3 plane of the $C_{24}F_{50}$ is given in Fig. 7. In order not to obscure the drawings, only the fit curves for certain temperatures are represented and measured data points are omitted. Figure 7 displays an inversion of the longitudinal sound velocities v_1 and v_3 (corresponding to c_{11} and c_{33}, respectively) already reported for $C_{16}F_{34}$ and $C_{20}F_{42}$ (Ref. 4) (s.a. below). In Figs. 8 and 9, we compare $c_{11}(T)$ and $c_{33}(T)$ for the three different perfluoroalkanes. As can be quantitatively seen from Table II, the temperature gradient of $c_{11}(T)$ is very similar among the three substances; there is no anomaly ob-

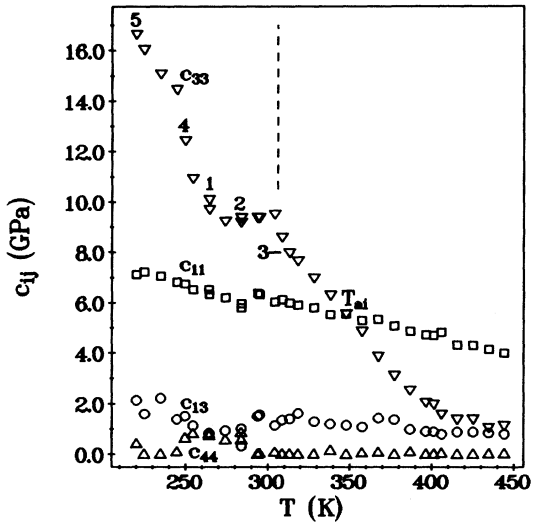

FIG. 6. Temperature dependence of the elastic stiffness coefficients c_{11}, c_{33}, c_{13}, and c_{44} of $C_{24}F_{50}$. T_{ai} is the anisotropy inversion temperature. The indices above some experimental data indicate the temperatures at which control measurements were performed (for further information see text). The vertical dashed line divides the two temperature regions discussed in the text.

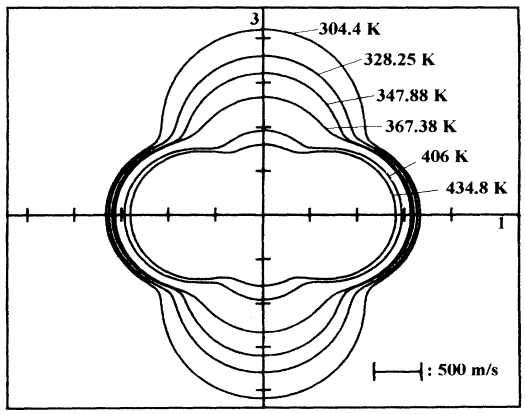

FIG. 7. Temperature evolution of the quasilongitudinal branch of the sound velocity polar plot in the 1–3 plane of $C_{24}F_{50}$. The stiffness values c_{11} and c_{33} can be calculated from the sound velocities measured along the 1 and 3 axes, respectively.

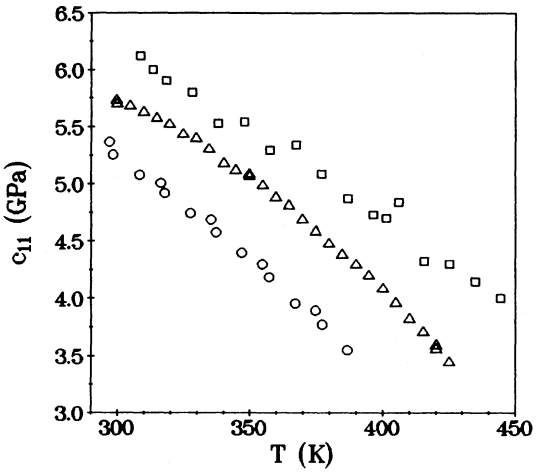

FIG. 8. Temperature dependence of c_{11} in the rotator phase above room temperature. Circles: $C_{16}F_{34}$. Triangles: $C_{20}F_{42}$. Squares: $C_{24}F_{50}$.

served until the melting temperatures (Fig. 8). Much more impressive is the behavior of $c_{33}(T)$ found for the three perfluoroalkanes as demonstrated by the large variation of the related temperature gradients (Table II and Fig. 9). However, these temperature gradients are still smaller than those observed for *n*-alkanes.[14,20] Comparing $c_{11}(T)$ and $c_{33}(T)$ (i.e., Fig. 6), one observes the interchange of the magnitudes of the longitudinal stiffness moduli at $T_{ai}=349$ K. In the model described in Ref. 4, we consider layers of stiff covalently bonded molecules separated by soft regions through which the neighboring layers are coupled by van der Waals forces. This "elastic series connection" is responsible for the elastic stiffness c_{33} which becomes clearly smaller than the stiffness c_{11} above T_{ai}. There is a further elastic anomaly at $T_2=398$ K characterized by a drastic change in slope of the $c_{33}(T)$

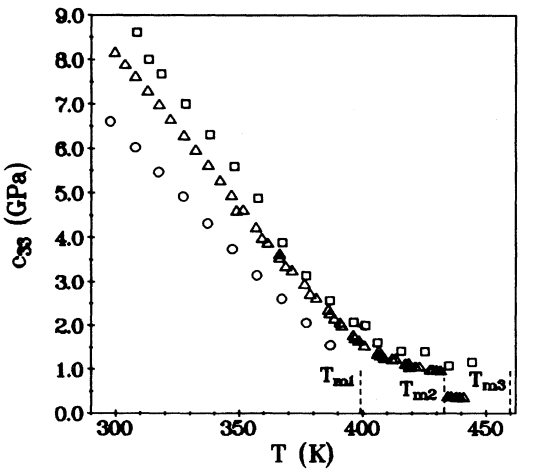

FIG. 9. Temperature dependence of c_{33} in the rotator phase above room temperature. Circles: $C_{16}F_{34}$. Triangles: $C_{20}F_{42}$. Squares: $C_{24}F_{50}$. The dashed lines mark the melting temperatures for $C_{16}F_{34}$ (T_{m1}), $C_{20}F_{42}$ (T_{m2}), and $C_{24}F_{50}$ (T_{m3}).

below the melting temperature. Comparing $C_{20}F_{42}$ and $C_{24}F_{50}$ (Table II), the premelting temperatures T_2 and the absolute values of c_{33} near the melting temperature are almost the same despite the difference in chain length. This fact is astonishing because the melting temperatures and phase transition temperatures within the solid state usually strongly depend on the molecular chain lengths. As a reference for the elastic behavior of perfluoroalkanes in the melt, we will use the values obtained for the elastic constant $c_m(T)$ in the melt of $C_{20}F_{42}$.[4] The corresponding temperature gradient is still lower than that of $c_{11}(T)$ and is also listed in Table II. The complicated temperature behavior of c_{11} and c_{33} allows the definition of several characteristic temperatures (Fig. 10, Table III); T_1 is given by the (hypothetical) intersection of $c_{33}(T)$ with $c_m(T)$ and is located below the melting temperature. The ultimate softening, $c_{33}=0$, would happen at $T_0<T_m$ if the Curie-Weiss-like behavior of $c_{33}(T)$ would not break down at T_2 due to the disordering of the lamellae stacking.[16]

The surprisingly strong decrease of the elastic stiffness c_{33} on raising the temperature could eventually be due to a structural relaxation process which, in turn, should be accompanied by a significant attenuation maximum. The marked softening of $c_{33}(T)$ with increasing temperature and the absence of any anomalous temperature behavior of the hypersonic attenuation, therefore suggest the existence of a phase transition behavior. In this sense the elastic data of $C_{20}F_{42}$ (Ref. 4) were interpreted to be the results of a bilinear coupling between a hypothetical order parameter η, and the corresponding strain, ε_3, obeying a Curie-Weiss-law behavior.[30] This seems to hold in the low-temperature region $T<T_2$ ($T_2=398$ K, see Table III) but not in the $T>T_2$ region of $C_{20}F_{42}$ and also of $C_{24}F_{50}$. A bilinear coupling would result in an increase of the elastic modulus on increasing the temperature for $T>T_2$ (Ref. 30) and such behavior is observed neither in $C_{20}F_{42}$ nor in $C_{24}F_{50}$. To try to explain the anomalous behavior of c_{33}, Dvorák and Holakovský[16] have proposed a phenomenological model in the frame of the Landau theory based on the destruction of the regular stacking of the lamellae of the form *ABC-ABC-*...[17] that builds up the telomer crystal. In this work, the order parameter η is related to the probability of finding a lamella *B* after a lamella *A* and a lamella *C* after a lamella *B*. The symmetry of such an order parameter implies that only the quadratic terms of the order parameter are allowed in the expansion of the free energy.[16] The elastic behavior is described by the coupling term $\eta^2\varepsilon_3$ where ε_3 is the strain component related to c_{33}. This coupling leads to a steplike anomaly $c_{33}(T)$ at a definite temperature T_c, which can be considered as an interlamellar melting point, giving rise to a statistically distributed hexagonal packing of *A*, *B*, and *C* lamellae. The experimental data of $c_{33}(T)$ present a change of slope rather than a step. In this phenomenological model, the suppression of the step is explained in terms of a pure dynamic effect related to the fact that the relaxation time τ of the ordering mechanism is much larger than ω^{-1} corresponding to the Brillouin experiment, i.e., $\omega\tau\gg1$. Then the change of slope of

TABLE II. Temperature gradients of $c_{11}(T)$, $c_{33}(T)$, and $c_m(T)$ in the temperature range between room temperature and the melting temperature T_m. In the case of $c_{33}(T)$ the temperature range $220 < T < 250$ K is added.

Temperature gradients in GPa/K	$C_{16}F_{34}$	$C_{20}F_{42}$	$C_{24}F_{50}$
$\frac{dc_{11}}{dT}$	−0.019±0.001	−0.018±0.001	−0.015±0.001
$\frac{dc_{33}}{dT}\Big\vert T < T_2$	−0.057±0.001	−0.069±0.001	−0.077±0.002
$\frac{dc_{33}}{dT}\Big\vert T > T_2$		−0.010±0.001	−0.011±0.005
$\frac{dc_{33}}{dT}\Big\vert T < 250$ K			−0.089±0.008
$\frac{dc_m}{dT}$		−0.002±0.001	

$c_{33}(T)$ might be due to a biquadratic term $\frac{1}{2}g\eta^2\varepsilon^2$ (g is the coupling constant), which below T_2, contributes to c_{33} by $g\eta_s^2(T) \sim g(T_2 - T)$ (η_s denotes the spontaneous value of the order parameter η) and could explain the increase of c_{33} with decreasing temperature below T_2 provided $g > 0$. The critical temperature T_2 would be the temperature at which the regular *ABC* stacking in the rotator phase is lost giving rise to an incomplete interlamellar melting. It is incomplete in the sense that the material remains solid, not transforming in a true smectic-*B* liquid crystal. Moreover, for $C_{20}F_{42}$ and $C_{24}F_{50}$ the temperature T_2 does not seem to be influenced by the chain length of the perfluoroalkane, indicating that the mechanism responsible for the softening of the longitudinal-acoustic mode c_{33} must be inherent in the definition of the interlamellar regions of the prefluoroalkane crystal.

The influence of the interlamellar regions in the elastic stiffness coefficient c_{33} can be immediately noticed when comparing the Raman spectroscopic measurements of the longitudinal-acoustic mode frequency (LAM) that allows the evaluation of the limiting elastic coefficient c_{33}^{LAM}. In the case of $C_{16}F_{34}$ and $C_{20}F_{42}$ the value of this elastic coefficient of a single lamella is almost the same, being $c_{33}^{\mathrm{LAM}} \approx 200$ GPa, and temperature independent.[4] Similar results were obtained in the case of linear *n*-alkanes.[1] Then it is clear, that the elastic properties along the crystallographic *c* axis of the rotator phase related to a series connection between covalent and van der Waals interactions are dominated by the latter. These van der Waals interactions take place between the end-groups of adjacent carbon chains, in this case fluorine atoms, and will be influenced by the onset of disorder in the rotator phase. The disorder of the rotator phase up to room temperature ($T \approx 300$ K) has been interpreted in terms of inter- and intramolecular types in the case of $C_{20}F_{42}$;[17–19] the similarity in the elastic behavior of $C_{20}F_{42}$ and $C_{24}F_{50}$ allows the use of this interpretation in the case of $C_{24}F_{50}$. The intramolecular disorder is related to the appearance of helix reversal defects in each molecule and to the tendency of the C_nF_{2n+2} molecules to achieve the all-trans conformation in the rotator phase [the all-trans conformation of the molecules can be related to the characteristic quantity u/t, monomer units per helix turns, when $u/t = 2$ (Ref. 18)]. In the case of intermolecular disorder, besides a disorder related to the onset of molecule rotations about their long axis, there exists disorder in the longitudinal position of the molecules. Both types of intermolecular disorder are intimately related to each other.[19] Due to the helix handedness of the molecules, the rotational disorder implies a longitudinal

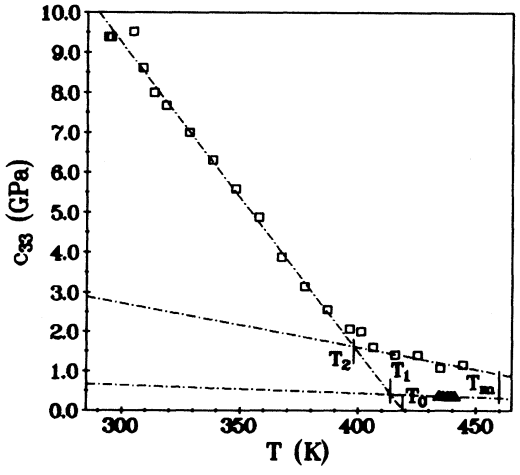

FIG. 10. Definition of the characteristic temperatures of $C_{24}F_{50}$ (see also Table III). To evaluate T_1 we used the elastic stiffness constants, c_m (triangles), of $C_{20}F_{42}$ in the melt.

TABLE III. Characteristic temperatures obtained from the experimental data of the elastic stiffness coefficients $c_{11}(T)$ and $c_{33}(T)$ of $C_{16}F_{34}$ (Ref. 4), $C_{20}F_{42}$ (Ref. 4), and $C_{24}F_{50}$. For further information see text.

	$C_{16}F_{34}$	$C_{20}F_{42}$	$C_{24}F_{50}$
T_m	399 K	434 K	459.6 K
T_0	414 K ($C_{20}F_{42}$ melt)	416 K	420.6 K ($C_{20}F_{42}$ melt)
T_1	406.3 K	409.7 K	415 K
T_2		398 K	398 K
T_{ai}	331 K	345 K	349 K

motion in the sense of a screw rotating in its thread. This coupled behavior leads to a roughening of the interlamellar regions with the corresponding strong decrease of the related elastic constant c_{33}. Only in the case of decoupling of both states of disorder, the elastic constant c_{33} would recover a temperature dependence similar to that expected for van der Waals interactions [i.e., similar to that of $c_{11}(T)$]. This decoupling process is indicated by the tendency of the molecules to adopt the all-trans conformation ($u/t=2$) at high temperatures. If we demand that at T_2 the molecules show the all-trans conformation, we obtain the diagram shown in Fig. 11. It is clearly seen that T_2 is a kind of critical temperature and we expect a smooth approach to $u/t=2$ at temperatures $T<T_2$. The invariance of T_2 can be understood only if the tendency to achieve an apparent all-trans conformation is independent of the number of carbons in the molecular chain. When u/t approaches 2, an increasing number of molecules contain helix defects (helix reversals) so that in average the helicity of the molecules is being lost gradually leading to a decoupling between rotational and longitudinal motions. We expect that the helix defects can shift along the molecular chain axis rather easily and hence, the correlation of positions of endgroups of each individual molecule is lost. Since the regular stacking of molecular layers implies definite positions of the molecular endgroups, we conclude that when $u/t=2$ at T_2, simultaneously the regular stacking is destroyed. In this context, we would expect also a change in the temperature behavior of the shear elastic constant c_{44}. The experimental values obtained for $c_{44}(T)$ are almost zero for $C_{20}F_{42}$ and $C_{24}F_{50}$ and the experimental accuracy does not allow the observation of any noticeable changes in its temperature dependence.

The resulting irregular stacking of the lamellae suggests the existence of a smectic-*B*-like phase as in liquid crystals. Indeed, the temperature behavior of c_{11} and c_{33} is very similar to that found for the liquid crystal 4-*n*-pentoxybenzylidene-4′-*n*-octoaniline (5O.8) (see Fig. 12 and Ref. 31). In the smectic-*B* phase of this liquid crystal $c_{11}>c_{33}$ holds, which is also observed in $C_{16}F_{34}$, $C_{20}F_{42}$, and $C_{24}F_{50}$ above and below T_2. Additionally, in the case of $C_{20}F_{42}$ and $C_{24}F_{50}$, the temperature gradients of c_{11} and c_{33} above T_2 are very similar (see Table II) and this is also observed in the smectic-*B* phase of 5O.8. The absolute value of the anisotropy in $C_{20}F_{42}$ and $C_{24}F_{50}$ is much bigger than in the case of 5O.8. From the elastic point of view, it turns out that the premelting phases of $C_{20}F_{42}$ and $C_{24}F_{50}$ ($T>T_2$) are not smectic-*B* phases because c_{44} is definitely nonzero although very small. This means, that the decoupling of the molecular lamellae remains incomplete.

IV. CONCLUSIONS

We have taken advantage of a new crystal-growth technique (PIA technique) allowing thus a quick and easy preparation of single-crystalline films of fluorinated *n*-telomers. The PIA technique also provides a preferential direction of the crystallites in the film plane having at least one crystallographic axis in the film plane. The Brillouin spectroscopy using the 90 *A*-scattering geometry permits the determination of the elastic constants of the prepared film that corresponds to a main crystal cut in the case of elastic hexagonal symmetry, as is the case of the investigated sample $C_{24}F_{50}$. The temperature dependence of the elastic constants shows the

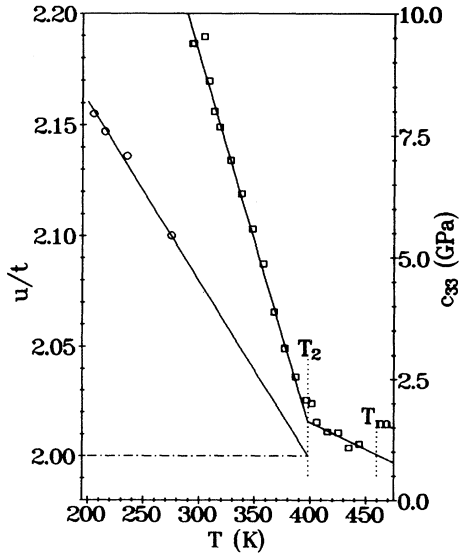

FIG. 11. Temperature dependence of c_{33} (squares) and of the helix parameter u/t (monomer units per helix turns) (circles). The c_{33} data correspond to $C_{24}F_{50}$. The u/t data correspond to the perfluoroalkane $C_{20}F_{42}$ (Ref. 18). $u/t=2$ (horizontal line) corresponds to an apparent all-trans conformation.

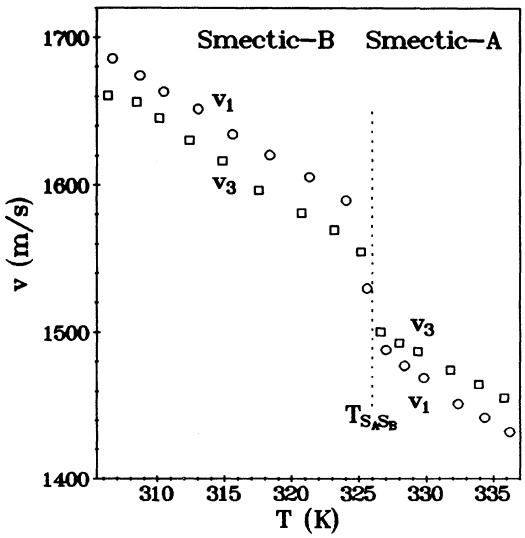

FIG. 12. Temperature behavior of the principal longitudinal sound velocities v_1 (circles) and v_3 (squares) around the smectic-*B*–smectic-*A* phase transition of the liquid crystal 4-*n*-pentoxybenzylidene-4′-*n*-octoaniline (5O.8). In the smectic-*A* phase one observes $c_{33}>c_{11}$. $T_{S_AS_B}$ gives the transition temperature from the smectic-*A* to the smectic-*B* phase.

existence of a metastable phase immediately below room temperature. Above room temperature, the elastic behavior is similar to the well-known behavior of $C_{20}F_{42}$. The soft-mode behavior of $c_{33}(T)$ has been analyzed in terms of a premelting phase transition at the temperature $T_2=398$ K. At this temperature an average all-trans conformation of the chain molecules is established, which in turn is accompanied by a destruction of the regular stacking of the molecular endgroups. From the elastic point of view, this premelting phase is very similar to the smectic-*B* phase in the liquid crystal 5O.8. A bilinear coupling model seems to be adequate to describe the anomalous temperature dependence of $c_{33}(T)$. This transition is smeared out and is related to the decoupling of the rotational disorder of the molecules from their longitudinal translational disorder. It would be of great interest to know whether the observed elastic anomalies in *n*-alkanes and partially fluorinated alkanes within their rotator phase are also due to the destruction of regular stacking and the incomplete decoupling of the molecular lamellae. Further investigations are in progress.

ACKNOWLEDGMENTS

The DSC equipment Netzsch DSC200 was placed at our disposal by NETZSCH Gerätebau GmbH. This work was kindly supported by the Deutsche Forschungsgemeinschaft.

[1]G. R. Strobl and R. Eckel, J. Polym. Sci. **14**, 913 (1976).
[2]B. Wunderlich and J. Grebowicz, Adv. Polym. Sci. **60/61**, 1 (1984).
[3]J. K. Krüger, in *Optical Techniques to Characterize Polymer Systems,* edited by H. Bässler (Elsevier, Amsterdam, 1989).
[4]A. Marx, J. K. Krüger, and H.-G. Unruh, Z. Phys. B **75**, 101 (1989).
[5]A. Marx, J. K. Krüger, A. Kirfel, and H.-G. Unruh, Phys. Rev. B **42**, 6642 (1990).
[6]R. Boistelle, in *Current Topics in Material Science,* edited by E. Kaldis (North-Holland, Amsterdam, 1980), Vol. 4.
[7]W. Pechhold, W. Dollhopf, and A. Engel, Acustica **17**, 61 (1966).
[8]D. Heyer, U. Buchenau, and M. Stamm, J. Polym. Sci. **22**, 1515 (1984).
[9]U. Buchenau, Solid State Commun. **32**, 1329 (1979).
[10]J. K. Krüger, H. Bastian, G. I. Asbach, and M. Pietralla, Polym. Bull. **3**, 633 (1980).
[11]J. K. Krüger, M. Pietralla, and H.-G. Unruh, Phys. Status Solidi A **71**, 493 (1982).
[12]A. Marx, J. K. Krüger, and H.-G. Unruh, Appl. Phys. A **47**, 367 (1988).
[13]J. K. Krüger, L. Peetz, and M. Pietralla, Polymer **19**, 1397 (1978).
[14]J. K. Krüger, M. Pietralla, and H.-G. Unruh, Colloid and Polymer Sci. **261**, 409 (1983).
[15]J. K. Krüger, A. Marx, L. Peetz, R. Roberts, and H.-G. Unruh, Colloid and Polymer Sci. **264**, 403 (1986).
[16]V. Dvorák and J. Holakovský, Ferroelectrics **145**, 23 (1993).
[17]H. Schwickert, G. Strobl, and M. Kimmig, J. Chem. Phys. **95**, 2800 (1991).
[18]T. Albrecht, H. Elben, R. Jaeger, M. Kimmig, R. Steiner, G. Strobl, B. Stühn, H. Schwickeert, and C. Ritter, J. Chem. Phys. **95**, 2807 (1991).
[19]T. Albrecht, R. Jaeger, W. Petry, R. Steiner, G. Strobl, and B. Stühn, J. Chem. Phys. **95**, 2817 (1991).
[20]R. Jiménez, J. K. Krüger, M. Prechtl, C. Grammes, and P. Alnot, J. Phys. Condens. Matter **6**, 10 977 (1994).
[21]J. C. Wittmann and P. Smith, Nature (London) **352**, 414 (1991).
[22]J. K. Krüger, M. Prechtl, P. Smith, S. Meyer, and J. C. Wittmann, J. Polym. Sci. B **30**, 1173 (1992).
[23]J. K. Krüger, M. Prechtl, J. C. Wittmann, S. Meyer, J. F. Legrand, and G. D'Asseza, J. Polym. Sci. B **31**, 505 (1993).
[24]C. Schorr, M.S., University of Saarbrücken, 1994.
[25]C. Grammes, Ph.D. thesis, University of Saarbrücken, 1994.
[26]J. K. Krüger, E. Sailer, R. Spiegel, and H.-G. Unruh, Prog. Colloid and Polym. Sci. **64**, 208 (1978).
[27]J. K. Krüger, L. Peetz, R. Siems, H.-G. Unruh, M. Eich, O. Herrmann-Schönherr, and J. H. Wendorff, Phys. Rev. A **37**, 2637 (1988).
[28]J. K. Krüger, R. Jiménez, K. P. Bohn, J. Petersson, J. Albers, A. Klöpperpieper, E. Sauerland, and H.-E. Müser, Phys. Rev. B **42**, 8537 (1990).
[29]B. A. Auld, *Acoustic Fields and Waves in Solids* (Wiley, New York, 1973).
[30]W. Rehwald, Adv. Phys. **22**, 721 (1973).
[31]J. K. Krüger, C. Grammes, R. Jiménez, K.-P. Bohn, J. Baller, C. Fischer, D. Rogez, and P. Alnot, Phys. Rev. E (to be published).